https://doi.org/10.5194/egusphere-2026-3274
Preprint. Discussion started: 19 June 2026


# Seasonal Seismic Velocity Variations in the Western Bohemian Massif Using Ambient-Noise Cross-Correlation

Sourav Mandal[1], Tomáš Fischer[1], and Bohuslav Růžek[2]

[1]Institute of Hydrogeology, Charles University, Albertov 6, 12843 Prague 2, Czech Republic.
[2]Institute of Geophysics of the Czech Academy of Science, Boční II/1401, 141 31 Prague 4, Czech Republic

**Correspondence:** Sourav Mandal (mandalso@natur.cuni.cz)

**Abstract.** Changes in surface and near-surface loads, such as temperature and precipitation, can perturb crustal stress and generate measurable responses, including triggered seismicity, transient strain, and seismic velocity changes. Quantifying these responses provides a means to track the spatiotemporal evolution of stress and its coupling to fault slip and subsurface fluid processes. Traditional approaches, relying on recurring earthquakes or controlled sources, are limited by poor repeatability and high operational cost. Ambient-noise–based imaging avoids these constraints by using fixed receivers and continuous records to enable near-continuous monitoring. Here, we investigate relative seismic velocity variations ($\delta v/v$) in the western Bohemian massif using four years of ambient-noise recordings from 20 stations. We estimate $\delta v/v$ in the 0.1–0.5 Hz band across three coda windows and evaluate potential environmental drivers using cross-correlation. The strongest seasonal $\delta v/v$ signal is observed for station pairs with interstation distances shorter than 20 km and azimuths of 60°-120°, indicating that path geometry and ambient-noise illumination strongly influence the stability of the measurements. Correlation estimates suggest that, $\delta v/v$ is primarily associated with thermoelastic strain driven by atmospheric temperature variations, while groundwater-level fluctuations may contribute a weaker secondary hydrological signal whose mechanism remains ambiguous.

## 1 Introduction

Crustal rocks are continually influenced by a variety of atmospheric and hydrological processes, including fluctuations in air pressure and temperature, precipitation, and variations in groundwater level. These external, non-tectonic forces can generate measurable elastic responses in the upper and mid-crust, often inducing seismic velocity changes (Sens-Schönfelder and Wegler, 2006; Meier et al., 2010) or, in some cases, the modulation and triggering of seismicity (Bettinelli et al., 2008; Liu et al., 2009). Understanding how these environmental loads perturb the crust is crucial for characterizing the temporal evolution of stress, assessing effective rheological properties, and distinguishing environmental effects from tectonic. Consequently, quantifying subsurface changes driven by environmental loading has become a key objective in observational seismology.

The emergence of ambient seismic noise interferometry has greatly advanced this effort; due to its continuous and ubiquitous nature, it provides an alternative to traditional techniques reliant on natural earthquakes (Poupinet et al., 1984; Peng and Ben-Zion, 2006) or costly active-source experiments (Li et al., 1998, 2006; Nishimura et al., 2000). Seasonal $\delta v/v$ variations derived from noise-based methods have commonly been linked to annual cycles in temperature (Meier et al., 2010; Hillers et al., 2015),

https://doi.org/10.5194/egusphere-2026-3274
Preprint. Discussion started: 19 June 2026


atmospheric pressure (Gradon et al., 2021), and precipitation (Sens-Schönfelder and Wegler, 2006). A single environmental driver may act through different mechanisms at different depths: for instance, rainfall may alter shallow elastic properties through pore-fluid infiltration (Berryman, 2007), while simultaneously imposing surface loads capable of perturbing crustal stresses at seismogenic depths (Bettinelli et al., 2008).

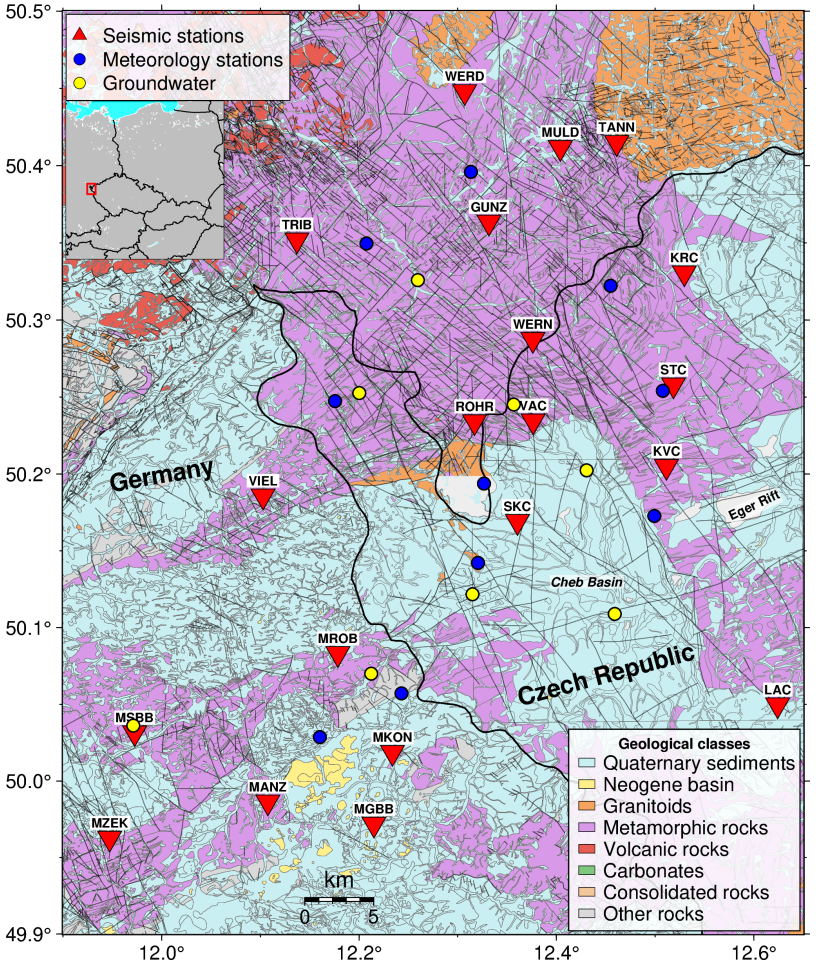


**Figure 1.** Geology map of the region showing the location of the seismic stations ( inverted red triangles), meteorology locations (blue circles), and groundwater locations (yellow circles). Geological data are from the Czech Geological Survey GeoCR50, the Saxony GK50 Erzgebirge/Vogtland service, and the Bavarian dGK25 dataset.

This study investigates temporal variations of seismic velocity in western Bohemia using four years of ambient seismic noise data and assesses whether any observed changes are linked to environmental forcing. We quantify $\delta v/v$ changes in the 0.1–0.5 Hz frequency band across three different coda windows, corresponding to increasing lag-times. We then examine the cross-correlation between $\delta v/v$ and key environmental variables, with the aim of identifying the dominant drivers of velocity fluctuations at different lag-times. To our knowledge, no previous study has quantified seasonal $\delta v/v$ variations within the

https://doi.org/10.5194/egusphere-2026-3274
Preprint. Discussion started: 19 June 2026


Bohemian Massif. More recently, Kramer et al. (2025) examined the relationship between $\delta v/v$ and air pressure at daily to sub-daily scales on a broader regional level, rather than at seasonal timescales.

## 2 Methodology and Data processing

We used the vertical component (Z) of continuous seismic noise recorded by a combination of eight broadband and twelve short-period stations with inter-station distances ranging from ∼4 km to ∼62 km (Fig. 1) covering a four-year period from January 2016 to December 2019.

We processed daily continuous seismic records using the Python package ObsPy (Beyreuther et al., 2010). The initial pre-processing steps include removal of the instrument response, detrending, demeaning and resampling the data to 20 Hz. We also filtered the data in the passband of 0.1-0.5 Hz. The relatively high sampling rate was retained to ensure robust temporal resolution. The data were then segmented into 1-hour windows. Cross-correlations were computed between ZZ components for all available preprocessed 1-hour segments between each of the 190 station pairs.

The removal of earthquake signals and instrumental noises from seismic data is crucial for obtaining meaningful and reliable results. These types of irregularities tend to compromise the quality of the seismic signal, leading to a spurious interpretation of the results. The quality of the cross-correlations was evaluated using the signal-to-noise ratio (SNR) defined by Clarke et al. (2011) as the ratio of the Hilbert envelope of a stacked signal $\langle cc(t)\rangle$,

$$s(N,t) = |\langle cc(t)\rangle + iH(\langle cc(t)\rangle)| \tag{1}$$

where $H(.)$ denotes the Hilbert transform of the stacked signal $\langle cc(t)\rangle$ and $i$ is the imaginary number; and the variation between each constituent signal $\langle cc(t)\rangle$, at each lag-time,$t$,

$$\sigma(N,t) = \sqrt{\frac{\langle cc(t)^2\rangle - \langle cc(t)\rangle^2}{N-1}} \tag{2}$$

$N$ is the number of signals that were stacked.

$$SNR(N,t) = \frac{s(N,t)}{\sigma(N,t)} \tag{3}$$

A higher SNR indicates clearer signal retrieval and better data quality. To remove the irregularities in the seismic signal and acquire cross-correlations with good SNR, we followed a two-step method. In the first step, we removed all pre-processed hourly segments whose energy (square of amplitude) exceeded 1.5 times the mean of energy over the entire day. In the second step, we rescaled the amplitude of the leftover signals by applying temporal normalization. In this step, we tested three different methods and checked their performance on SNR. The first method is running-absolute-mean normalization, which calculates the running average of the absolute value of a selected time window of fixed length and weights at the centre of the waveform window by the inverse of the average (Bensen et al., 2007; Yang et al., 2007). The second method, '1-bit' normalization, has been used in a number of ambient noise studies (Schimmel et al., 2011; Takano et al., 2014 ), which artificially modifies the seismogram by changing the positive and negative amplitude values of the data stream to +1 and -1, respectively. However,

https://doi.org/10.5194/egusphere-2026-3274
Preprint. Discussion started: 19 June 2026


this crude clipping process produces high-frequency noise and causes artificial modification of the ambient noise spectrum (Sabra et al., 2005). In the third method, amplitudes are clipped at a specified number of standard deviations from the mean of the amplitudes in each window (Sabra et al., 2005; Poli et al., 2012; Zigone et al., 2015). Among the tested normalization approaches, clipping amplitudes at four standard deviations from the mean produced the highest root-mean-square SNR and was therefore used for the final processing. This two-step procedure was used to remove high-energy transient windows while

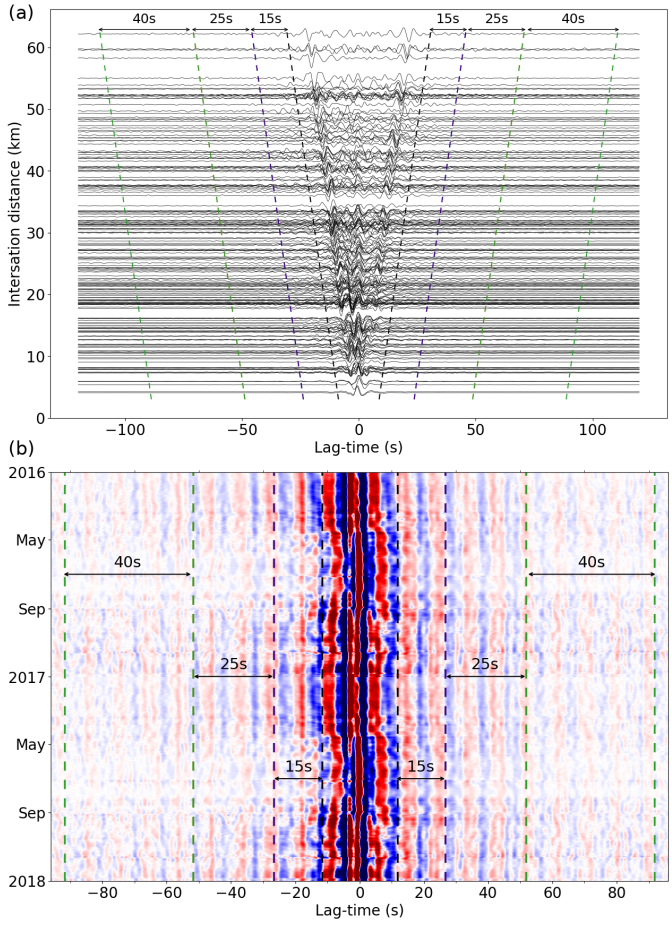


**Figure 2.** (a) Cross-correlation functions, stacked over the whole data period, ordered by inter-station distance. Each color line bracket represents the coda windows used for the velocity calculations. (b) 2-yr 2D correlogram for the station pair VAC–KVC (azimuth : 108.93°, inter-station distance : 10.15 km), where each daily correlation is formed by stacking 1-hour correlations within a ±7-day window. The Figure also shows the coda windows and their corresponding window lengths used for the $\delta v/v$ calculations.

limiting the influence of remaining amplitude outliers. We also spectrally whitened the data to the target frequency band 0.1-0.5 Hz.

For each pair, the hourly cross-correlations were stacked to form multi-day averages using a ±7-day stacking window (for example, for Julian day 156, hourly data from days 149–163 were stacked). Reference cross-correlation functions (CCFs) were

https://doi.org/10.5194/egusphere-2026-3274
Preprint. Discussion started: 19 June 2026


obtained by stacking all available hourly correlations over the entire four-year period (Fig. 2a). We then estimated relative seismic velocity variations $\delta v/v = -\delta t/t$ using the stretching technique (Lobkis and Weaver, 2003; Wegler and Sens-Schönfelder, 2007) with the help of the Python program NoisePy (Jiang and Denolle, 2020). In this method, the current waveform ( $\phi_{cur}$ ) is positively or negatively stretched in time to find the highest similarity (correlation coefficient, CC) with the reference waveform ($\phi_{ref}$) ( Lobkis and Weaver, 2003; Wegler and Sens-Schönfelder, 2007 ):

$$CC(\epsilon) = \frac{\int \phi_{ref}(t)\phi_{cur}(t\{1+\epsilon\})dt}{\sqrt{\int \phi^2_{ref}(t)dt \int \phi^2_{cur}(t\{1+\epsilon\})dt}} \tag{4}$$

Then the relative variation is determined by the stretching factor $\varepsilon$ for which the similarity between the stretched current waveform and the reference waveform is maximum. The analysis was restricted to the coda portion of the cross-correlation functions, which is more stable against variations in noise source distribution compared to direct arrivals (Colombi et al., 2014). Three different non-overlapping coda lapse time windows, as shown in Figure 2, were selected to sample different lapse-time portions of the scattered wavefield. Later coda windows are expected to contain more multiply scattered energy and may have broader effective spatial sensitivity (Obermann et al., 2013), although they should not be interpreted as independent depth levels. We used different window lengths for each coda window: 15 s for the first, and 25 and 40 s for the second and third, respectively. The reason to consider longer windows in later periods was to incorporate more waves in later coda windows, as the scattered waves tend to decay as they travel further through the media. We separately applied the stretching technique to the causal and acausal parts of the cross-correlation functions, then averaged the computed delay times and correlation values. All the delay times with correlation coefficient less than 0.7 were excluded from further analysis. To evaluate pair-to-pair variability, we calculated the daily standard deviation of $\delta v/v$ across all contributing station pairs for each coda window. This calculation was performed separately for the full network and for the path-selected subset and is used as a descriptive measure of station-pair variability.

## 3 Results

### 3.1 Observed relative velocity variations

Relative seismic velocity changes, $\delta v/v$, were estimated from ambient-noise cross-correlations in the 0.1–0.5 Hz band using the stretching method and then averaged across 190 station pairs to produce a record spanning early 2016 through late 2019 (Fig. 3a). The results are shown for three different coda windows as indicated in Figure 2, corresponding to early, middle, and late portions of the coda wavefield. Each coda window represents a different segment of the scattered wave energy, offering varying sensitivity to structural changes at various depths and spatial scales.

Averaged over all station pairs during the four-year monitoring period, the $\delta v/v$ variations for the whole network remain largely stable, with seasonal fluctuations typically contained within $\pm 0.35$ per cent (Fig. 3a). The full-network average shows no obvious long-term monotonic drift or permanent offset during the four-year period. Instead, the dominant variability is seasonal, with generally higher $\delta v/v$ values during warmer months and lower values during winter. Following each seasonal

https://doi.org/10.5194/egusphere-2026-3274
Preprint. Discussion started: 19 June 2026


cycle, $\delta v/v$ consistently returns to its baseline level, implying that the crust did not experience any lasting structural changes during the studied period. Instead, the velocity fluctuations reflect reversible stress perturbations associated with periodic environmental forcing rather than permanent damage, fault-zone alteration, or progressive tectonic deformation. The three coda windows, representing early, middle, and late lapse times, show strong temporal coherence, with the first window generally exhibiting slightly larger amplitude variations. The $\delta v/v$ signal exhibits a clear seasonal cycle, with velocities increasing during the warmer summer months and decreasing during the winter months. Peak seasonal amplitudes range from approximately $+0.1$ per cent to $+0.2$ per cent, and minima fall between $-0.1$ per cent and $-0.15$ per cent, with the strong seasonal signal observed in the summers of both 2018 and 2019.

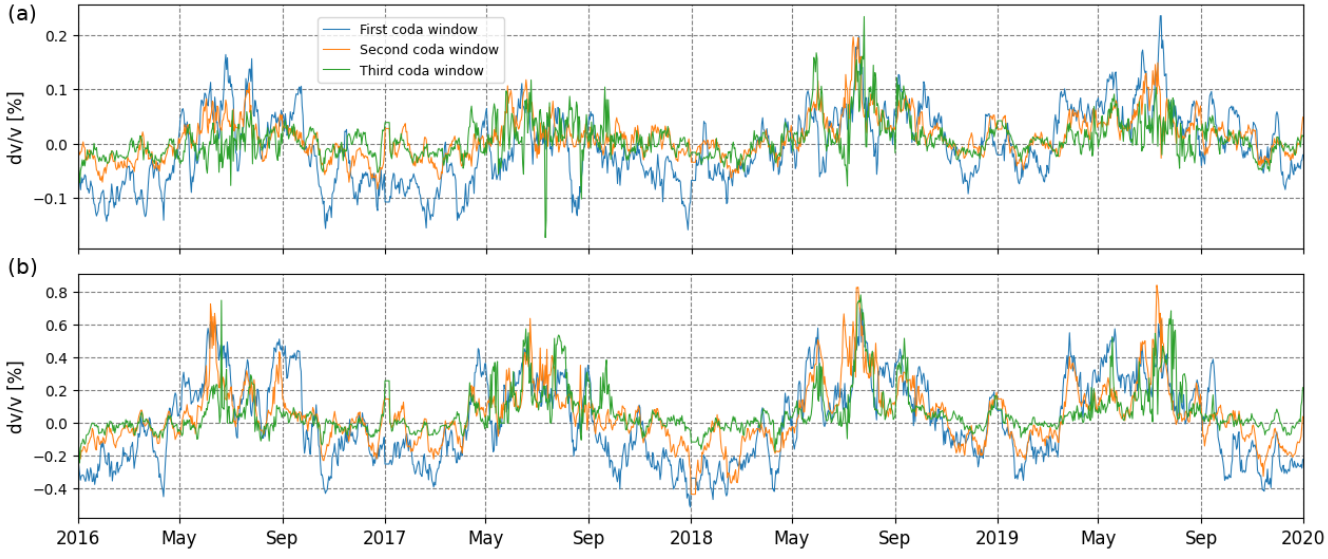


**Figure 3.** Relative velocity variations estimated in the 0.1–0.5 Hz band for the three coda windows. (a) Mean $\delta v/v$ averaged over all station pairs. (b) Mean $\delta v/v$ averaged over the path-selected subset with interstation distance $< 20$ km and azimuth 60-120 degrees. Pair-to-pair variability, estimated from the daily standard deviation across contributing station pairs, is shown in Fig. S1.

We further investigate the dependence of $\delta v/v$ on the interstation pair distance. When $\delta v/v$ results are separated into 20 km interstation distance bins, only station pairs shorter than 20 km exhibit a strong and repeatable seasonal cycle (Fig. S2). Pairs between 20 and 62 km display weaker or incoherent signals with no consistent annual pattern. This loss of clarity in longer pairs is likely due to a combination of path averaging, reduced near-surface sensitivity, and attenuation effects. Longer interstation paths sample a broader and more heterogeneous crustal volume, diminishing the seasonal signal, as well as reduced sensitivity to shallower changes and lower cross-correlation stability. In addition, geometrical spreading, intrinsic attenuation, and scattering attenuation progressively reduce the amplitude of the coda wavefield with increasing propagation distance. This distance-dependent amplitude loss has been observed in ambient-noise correlations, where surface-wave amplitudes decay with receiver separation and require attenuation terms in addition to geometrical spreading (Weemstra et al., 2013). More generally,

https://doi.org/10.5194/egusphere-2026-3274
Preprint. Discussion started: 19 June 2026


coda-wave amplitudes are controlled by both intrinsic absorption and scattering from crustal heterogeneities (Aki and Chouet, 1975; Sato et al., 2012). Consequently, weaker long-distance correlations may have lower signal-to-noise ratios and reduced temporal stability, making small seasonal dv/v variations more difficult to recover reliably (Bensen et al., 2007; Stehly et al., 2007).

Similarly, we separate the results by azimuth. When the network is analyzed by azimuth in $30^\circ$ bins for all three coda windows, only pairs oriented between $60^\circ$ and $120^\circ$—roughly east–west—exhibit strong, coherent seasonal cycles (Fig. S3). This directional dependence can be explained by the anisotropy of the ambient seismic noise field in Central Europe. At the studied frequency range (0.1–0.5 Hz), the dominant energy is associated with secondary microseisms generated by North Atlantic storms, which propagate toward the continent in a predominantly west-to-east direction (Friedrich et al., 1998; Stehly et al., 2006 ). East–west oriented station pairs are therefore better aligned with the incoming wavefield, resulting in stronger and more coherent cross-correlations, whereas paths at other azimuths sample the noise field less effectively and suffer from lower signal-to-noise ratios.

When both filters are applied—restricting the dataset to pairs shorter than 20 km and oriented between $60^\circ$ and $120^\circ$—the seasonal $\delta v/v$ cycle becomes substantially clearer than in the full network average (Fig 3b). The annual cycle is more sharply resolved, with more consistent seasonal maxima and minima and less scatter around the dominant trend. This indicates that the selected subset contains the station pairs with the most stable and coherent velocity estimates. Short interstation distances likely enhance sensitivity to shallow crustal variations, where seasonal forcing is strongest, while reducing path-averaging effects that can obscure coherent $\delta v/v$ changes along longer paths. The favourable azimuth range further suggests that these paths are better aligned with the dominant ambient-noise field, producing more stable cross-correlations. This path-selected subset is therefore used as the primary dataset for the environmental analysis below. Importantly, the selection is based on the distance- and azimuth-dependent stability tests described above, rather than on the subsequent correlations with environmental variables; robustness tests using nearby distance and azimuth selections are provided in Table S1.

### 3.2 Spectral content in the observed velocity changes

We perform a power spectral density (PSD) analysis of $\delta v/v$ for the filtered subset of station pairs (distance $< 20$ km, azimuth $60^\circ$-$120^\circ$) for each coda window (Fig. 4). All three PSDs reveal a dominant peak corresponding to a period of approximately 365.25d, consistent with the strong annual cycle observed in the time domain (Fig. 3b). Secondary peaks are also evident, including $\sim$182d in all coda windows, $\sim$104d in the first and second windows, and $\sim$43d in the second and third windows. The dominant annual component reflects seasonal forcing, while the secondary peaks may indicate sub-annual cycles, potentially linked to hydrological or atmospheric loading patterns, or harmonics of the annual cycle. The recurrence of annual and sub-annual peaks across the three coda windows suggests that the seasonal signal is robust and not confined to a single lapse-time range.

https://doi.org/10.5194/egusphere-2026-3274
Preprint. Discussion started: 19 June 2026


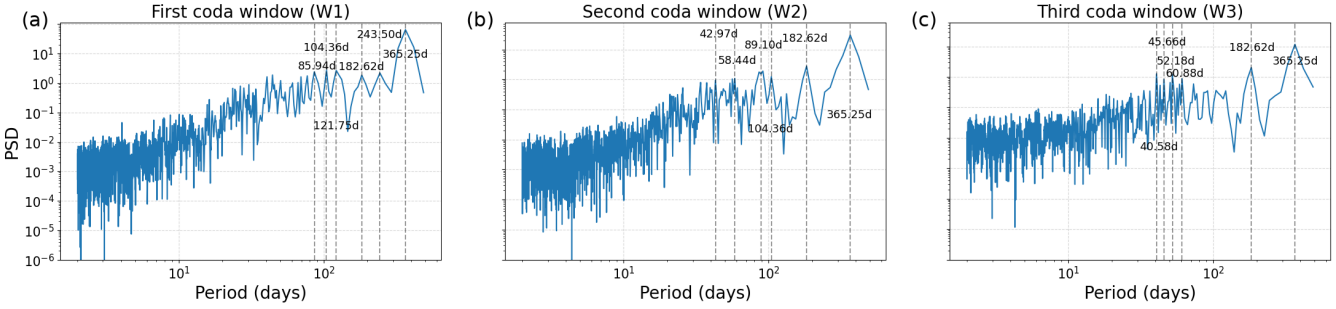


**Figure 4.** Power spectral density (PSD) of the subset $\delta v/v$ results shown in Fig. 3b for each coda window. The labelled vertical dashed lines mark the periods of the six highest PSD peaks in each window.

### 3.3 Depth sensitivity analysis

Under conditions of multiple scattering, wave propagation effectively follows a random-walk process and can therefore be accurately modeled by the diffusion equation (Pacheco and Snieder, 2005; Planès et al., 2014). In such scattering regimes, the three coda windows used for our $\delta v/v$ analysis contain both body and surface waves (Hennino et al., 2001). Obermann et al. (2013) showed that the partitioning between these wave types depends on lag time and on the scattering properties of the medium, commonly expressed through the scattering mean free path $l$ and the transport mean free path $l^*$. The parameter $l$ quantifies the average distance a wave travels before encountering a heterogeneity that scatters it, whereas $l^*$ represents the distance over which the wave effectively loses memory of its initial propagation direction. Both quantities are frequency dependent and related as:

$$l^* = \frac{l}{1 - \langle cos\theta \rangle} \tag{5}$$

with $\langle cos\theta \rangle$ as the directional average of the cosine of the scattering angle ($\theta$). However, under the assumption of isotropic scattering they become equivalent, such that $l^* = l$ (Obermann et al., 2013; Gaebler et al., 2015).

Following the formula, $l^* = 107(\frac{f}{Hz})^{-0.24}$ km, from Gaebler et al. (2015), we compute $l^*$ for our central frequency of 0.3 Hz and obtain a value of approximately 142.85 km. Using this value, together with a bulk wave velocity of 4.5 km/s and the central lag times of the three coda windows, we derive ratios of lag time to transport mean free time of 0.71, 1.46, and 2.48. According to Obermann et al. (2013), body-wave sensitivity becomes dominant only when this ratio exceeds 6. Our values are well below this threshold, indicating that the $\delta v/v$ measurements in this study are primarily controlled by surface-wave sensitivity. Because ZZ correlations are used, we further assume that Rayleigh waves dominate the coda wavefield (Margerin et al., 2009). Employing a recent 1-D velocity model for the western Bohemian region (Malek et al., 2023), we estimate, using the Python program DISBA, that the frequency band of 0.1–0.5 Hz sampled in this study is most sensitive to structural changes occurring at depths of roughly 2–6 km (Fig. S4).

Although the three coda windows correspond to increasing lapse times, they should not be interpreted as three independent depth levels. The ratios estimated above indicate that all windows remain below the body-wave-dominated regime and

https://doi.org/10.5194/egusphere-2026-3274
Preprint. Discussion started: 19 June 2026


are therefore primarily controlled by surface-wave sensitivity. Consequently, the later coda windows are interpreted here as sampling more scattered and spatially broader portions of the wavefield, with a possible but not uniquely resolved increase in effective depth sensitivity. The depth range inferred from the Rayleigh-wave kernels therefore provides an approximate

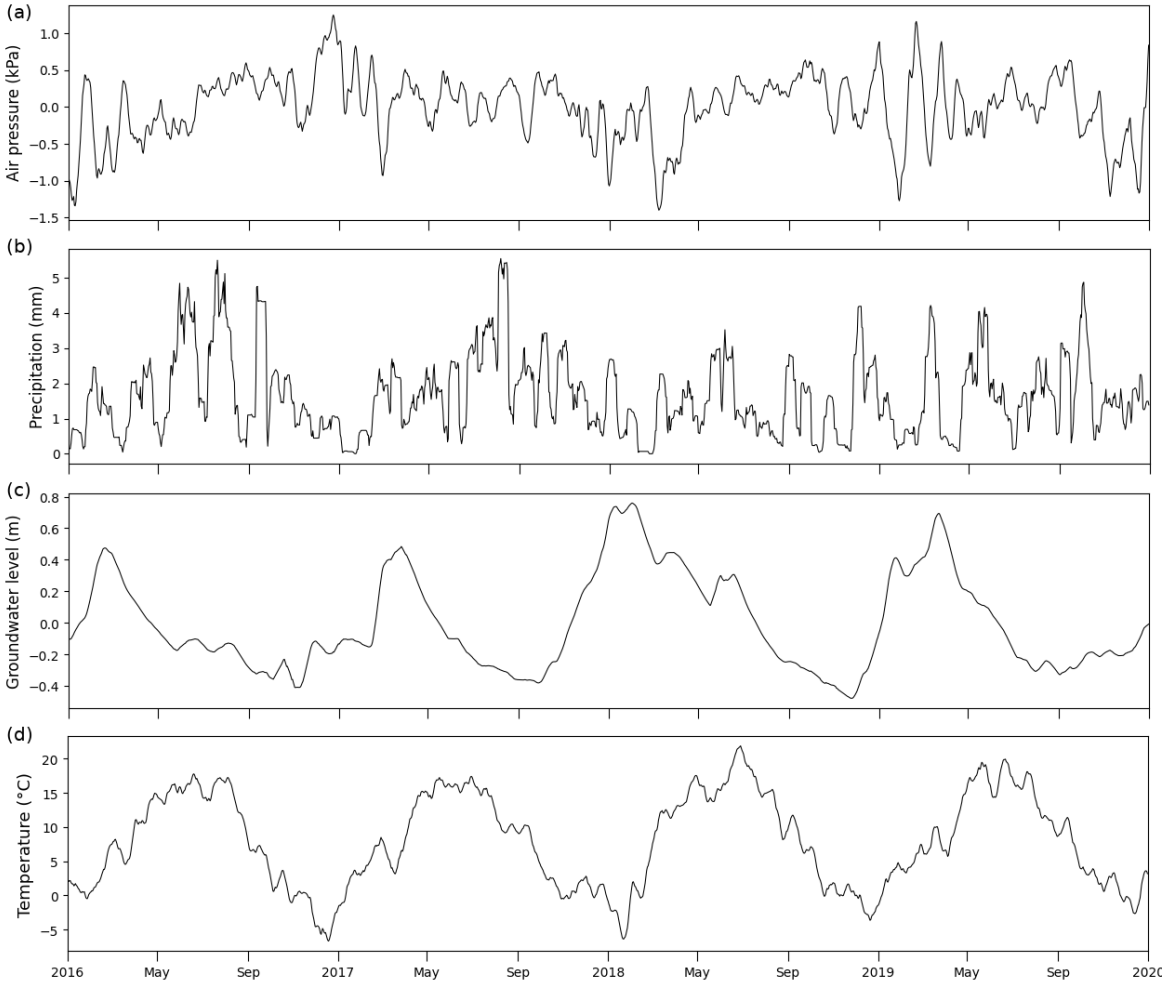


**Figure 5.** Daily meteorological and hydrological records used in the environmental correlation analysis: (a) atmospheric pressure, (b) precipitation, (c) groundwater level, and (d) air temperature. A 14-day smoothing window was applied to each record.

sensitivity range for the 0.1–0.5 Hz measurements, rather than a strict depth assignment for each coda window.

## 4 Analysis of possible environmental source mechanisms

Seismic velocity variations ($\delta v/v$) are known to be sensitive to a range of environmental factors, each of which modifies crustal elasticity through a distinct physical mechanism. Although these drivers often share similar seasonal periodicities, their pathways of influence differ fundamentally. Surface temperature affects $\delta v/v$ through thermoelastic expansion and contraction

https://doi.org/10.5194/egusphere-2026-3274
Preprint. Discussion started: 19 June 2026


of the upper crust, producing predictable seasonal stress changes that alter seismic wave speeds (Meier et al., 2010; Tsai, 2011). Atmospheric pressure imposes a poroelastic load on the ground surface, transferring stress into the pore-fluid network and modulating elastic properties according to near-surface permeability and compressibility (Niu et al., 2008). Precipitation and groundwater fluctuations influence $\delta v/v$ through hydrologic processes—changing pore pressure, saturation, and crack volume—often with delayed responses controlled by infiltration, diffusion, and aquifer geometry (Tribaldos and Ajo-Franklin, 2021).

As these mechanisms operate on different timescales and penetrate the crust to varying depths, the environmental contribution to $\delta v/v$ generally manifests as a superposition of thermal, poroelastic, and hydrological effects. Understanding their influence is essential for correctly interpreting the changes in $\delta v/v$ in regions. In the following, we examine how each environmental factor contributes to variations in $\delta v/v$ by cross-correlating $\delta v/v$ with each environmental factor within each coda window, providing a framework for assessing the dominant mechanisms that modulate seismic velocity changes in the study area. Because several environmental variables contain strong annual components, the correlation results are interpreted together with lag consistency, signal polarity, robustness to path selection, and physical plausibility rather than as independent proof of causality. The environmental analysis is performed primarily on the high-stability subset identified from distance and azimuth diagnostics. To test whether the interpretation depends strongly on this exact selection, we repeated the correlation analysis for alternative nearby path selections. For W1, the dominant temperature correlation and associated lag remain stable across these tests (Table S1); similar behaviour was also observed for W2 and W3, although with slightly weaker correlations.

### 4.1 Air pressure

Changes in air pressure act as a variable surface load on the Earth, a phenomenon well established in other fields of geoscience, such as geodesy and solid-Earth modelling (vanDam and Wahr, 1987; vanDam et al., 1994; Petrov and Boy, 2004). This load is then transmitted deeper into the crust, producing stress perturbations on the order of kPa. Because seismic velocities are stress-sensitive, the transmitted stress perturbs the seismic velocities in the media by modifying the compliant material discontinuities, also known as “cracks”. These cracks have been found even deeper into the crust, around 9 km (Huenges et al., 1997). Loading (increasing pressure) tends to close the cracks, increasing the contact area and contact stiffness at asperities; the crack network becomes less compliant, resulting in effective bulk and shear moduli that increase the seismic velocity. Unloading does the opposite: cracks reopen, compliance grows, moduli drop, and velocity decreases. This was observed by Niu et al. (2008), who noted an increase in seismic velocity resulting from an increase in air pressure.

Cross-correlations between atmospheric pressure variations and $\delta v/v$ in the 0.1-0.5 Hz band show a coherent but moderate-amplitude pattern (Fig. 6a). This pattern is consistent across all three coda windows. The magnitude of the correlation is significantly weaker than that associated with temperature or groundwater, but slightly higher than that associated with precipitation. These results indicate that although atmospheric pressure may contribute to seasonal $\delta v/v$ variability, it is not the dominant driver.

https://doi.org/10.5194/egusphere-2026-3274
Preprint. Discussion started: 19 June 2026


## 4.2 Precipitation

It has been observed that a change in seismic velocity due to precipitation can be explained via two mechanisms: first, when rainwater infiltrates pores and cracks. The infiltration of water into the open pore spaces alters both the bulk modulus and density of the saturated frame and changes the crack compliance (Berryman, 2007). In cracked/weakly consolidated media, the addition of water can decrease seismic wave speeds by opening compliant cracks and increasing attenuation/dispersion

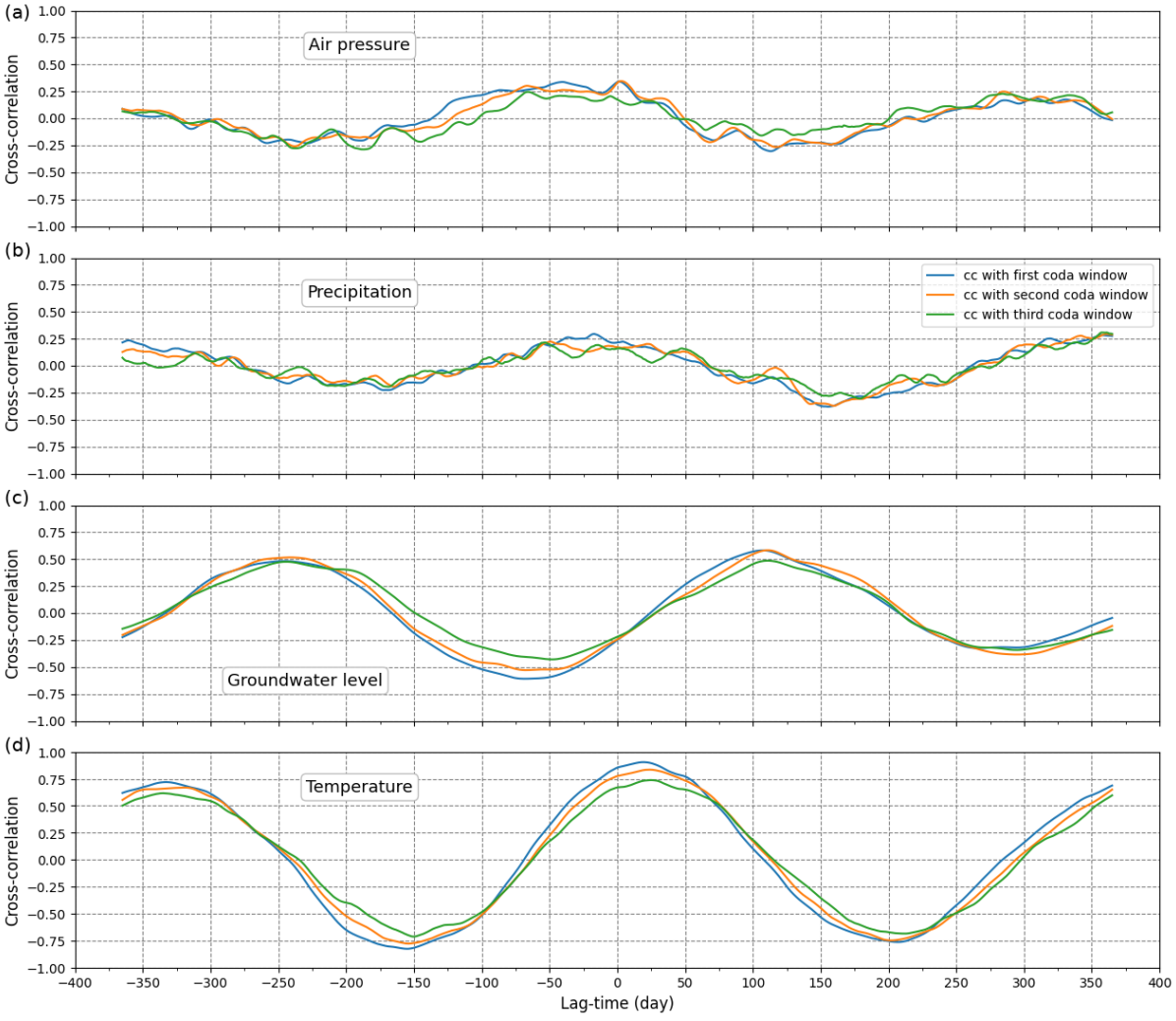


**Figure 6.** Cross-correlation estimates between the $\delta v/v$ results shown in Fig. 3b and environmental variables: (a) atmospheric pressure, (b) precipitation, (c) groundwater level, and (d) air temperature. Positive lag times indicate that $\delta v/v$ lags the environmental signal.

(Adam and Otheim, 2013; Li et al., 2020). These effects, however, are limited to shallow layers in which the groundwater level fluctuates (Sens-Schönfelder and Wegler, 2006; Meier et al., 2010). Secondly, accumulated rainfall exerts an additional

https://doi.org/10.5194/egusphere-2026-3274
Preprint. Discussion started: 19 June 2026


load on the surface, which can induce changes in poroelastic stress beneath the reservoir (Sens-Schönfelder and Wegler, 2006), additionally modulating the stress condition of the surrounding rock and the seismic velocity (Tsai, 2011).

In our study, the recorded rainfall is substantially low, with precipitation exceeding 20 mm during only a few days over our 4-year study period (Fig 5b). The correlation results between precipitation and $\delta v/v$ across all three windows exhibit very weak, noisy correlations (Fig. 6b). This behaviour demonstrates that precipitation does not appear to exert a direct, immediate influence on $\delta v/v$, and that short-term rainfall events do not appear to generate measurable elastic changes in the crustal depth range considered here. Based on these observations, precipitation is unlikely to be a primary driver of the observed $\delta v/v$ changes.

### 4.3 Groundwater level

On the other hand, fluctuations in groundwater level have a more direct effect on the seismic wave speeds compared to precipitation (Hillers et al., 2015). An increase in the groundwater table results in an increase in pore pressure in the area of direct fluid communication (Tribaldos and Ajo-Franklin, 2021), which leads to the opening of cracks and a decrease in grain contact area, thereby reducing seismic velocity (Christensen and Wang, 1985). Generally, stress disturbances produced by underground pore pressure have a negative correlation with $\delta v/v$ (Wang et al., 2017; Andajani et al., 2020). This effect is pronounced at shallow depths, around tens of meters below the surface and decreases as depth increases. However, an indirect cause, hydrological loading, has been observed to produce seasonal stress ( 2-4 kPa) variations at a depth range of approximately 10 km (Bettinelli et al., 2008). This should have the same effect as the additional load on the surface exerted by precipitation. This should exert a positive effect on $\delta v/v$; in other words, hydrological loading should give rise to a positive correlation between groundwater table fluctuation and $\delta v/v$.

The groundwater level record in our study depicts consistent oscillatory groundwater recharge and discharge during winter and summer periods, respectively, with the minima reached during the autumn months of 2018 (Fig. 5c). This reflects water storage deficits resulting from the massive droughts that occurred during the summers of these two years in Central Europe (Boergens et al., 2020). We also observed groundwater recharge at the beginning of 2018 and 2019, attributed to winter precipitation and snowmelt. Cross-correlating groundwater-level fluctuations with $\delta v/v$ in the 0.1–0.5 Hz band reveals a strong annual pattern (Fig. 6c). The correlation peaks at large positive lags, indicating that groundwater changes systematically lead the $\delta v/v$ response by roughly four months. The association is positive and reaches a maximum correlation of approximately 0.64. The positive polarity of this correlation suggests that the observed groundwater-related signal is unlikely to be explained solely by direct pore-pressure increase in shallow cracks, which would generally be expected to reduce seismic velocity. Instead, the positive correlation is more consistent with an elastic-loading contribution, in which increased water storage enhances normal stress and promotes crack closure. However, the large positive lag of approximately four months is difficult to reconcile with a purely elastic-loading response, which should be nearly instantaneous. Therefore, the groundwater correlation is interpreted as a secondary and physically ambiguous hydrological signal, potentially reflecting a combination of elastic loading, delayed hydraulic diffusion, and seasonal covariance with other environmental variables.

https://doi.org/10.5194/egusphere-2026-3274
Preprint. Discussion started: 19 June 2026


### 4.4 Temperature

Changes in atmospheric temperature have a direct effect on seismic velocities, as temperature changes also alter the elastic moduli. This direct effect of thermal diffusion, however, is limited only to the upper few meters of the crust. On the other hand, Ben-Zion and Leary (1986) and later Prawirodirdjo et al. (2006) have indicated that spatial differences in surface temperature or in the thermal properties of the heated material generate thermoelastic strain, which can propagate deeper into the crust. Ben-Zion and Leary (1986) also noted that the generated thermo-elastic strain is over ten times more potent than the effect of 15m changes of water level in a reservoir. Ben-Zion and Allam (2013) demonstrated stress levels exceeding 10 kPa in the top kilometre and approximately 2.4 kPa at a depth of 3 km, using simple calculations based on an annual temperature change of 20 °C and a spatial wavelength of 10 km. Meier et al. (2010) suggested that thermoelastic strain variation may be a reason for their observed seasonal seismic variation up to a depth of 15-22 km.

Atmospheric temperature variations in the western Bohemian region during the study period are dominated by a pronounced annual cycle (Fig. 5d). Temperature shows the strongest and most coherent cross-correlation with $\delta v/v$ among all environmental variables (Fig. 6d), indicating that $\delta v/v$ responds systematically to seasonal thermal variations. The correlation functions exhibit well-defined positive-lag maxima occurring approximately 19 to 25 days after temperature changes, which closely matches the 20-day delay previously reported by Hillers et al. (2015). This characteristic timescale is compatible with a thermoelastic origin: surface temperature anomalies propagate downward by thermal diffusion, producing thermoelastic stress perturbations in the shallow crust that modulate seismic velocities. The finite diffusion time to the depth range of maximum coda sensitivity, therefore, yields a delayed $\delta v/v$ response on the order of days to weeks. Collectively, the observed lag supports an interpretation in which the $\delta v/v$ signal is primarily driven by thermoelastic strain in the uppermost subsurface, consistent with expected thermal diffusivities for common near-surface lithologies.

Additional support for a thermoelastic origin comes from the lack of comparable coherence between $\delta v/v$ and other environmental variables. Precipitation and air pressure exhibit weaker and less stable correlations with $\delta v/v$. Groundwater level shows a secondary lagged correlation, but its positive polarity and long delay make the underlying mechanism less straightforward than the temperature response. These factors, therefore, cannot account for the robust seasonal pattern observed in $\delta v/v$, nor for the consistent time lag relative to temperature. Taken together, the strong coherence, well-defined lag, and physical plausibility of the thermoelastic model point to atmospheric temperature variations as the dominant driver of the $\delta v/v$ changes observed in the western Bohemian region.

### 4.5 Directional noise intensity

Beyond the environmental factors discussed above, variations in the spatial and temporal distribution of ambient-noise intensity, B, may also bias traveltime estimates when the noise field is nonisotropic or nonstationary (Yao and van der Hilst, 2009; Froment et al., 2010). Such changes in wavefield directionality can therefore produce apparent $\delta v/v$ fluctuations, even in the absence of a genuine seismic velocity change within the medium. This effect is expected to be more pronounced for direct waves than for coda waves, because multiple scattering progressively randomises propagation directions and makes the coda

https://doi.org/10.5194/egusphere-2026-3274
Preprint. Discussion started: 19 June 2026


wavefield more isotropic (Colombi et al., 2014). To assess this potential source of bias, we estimated the azimuthal distribution of noise intensity, $B(\theta)$, following the approach of Hillers et al. (2013), using the correlation SNR parameterisation of Larose et al. (2007). We computed $B(\theta)$ using the correlation stacks corresponding to summer (June-August) and winter (December-February) months.

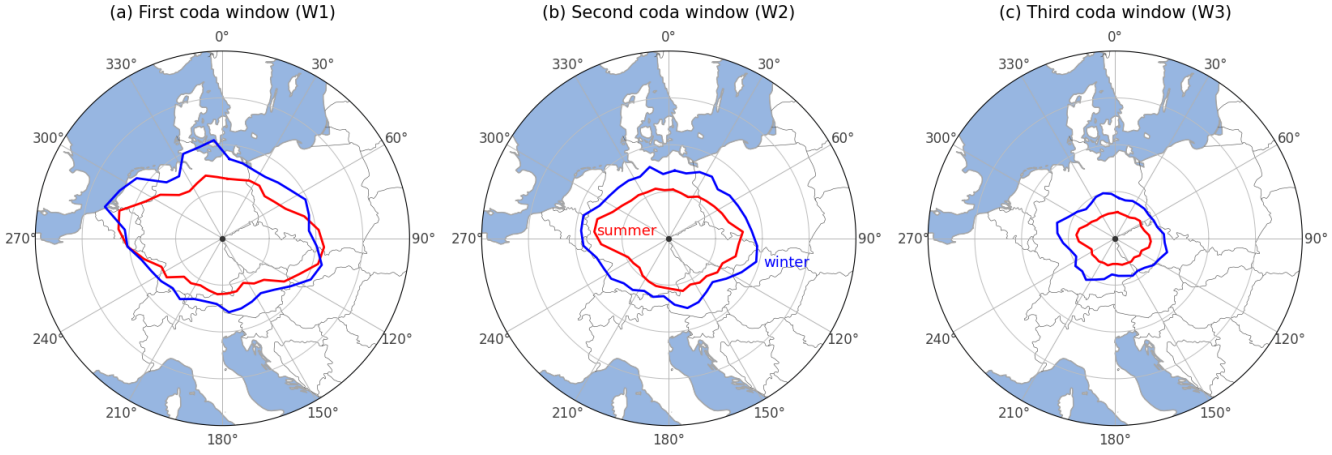


**Figure 7.** Noise intensity distributions, $B(\theta)$, for each coda window, inferred from azimuthal SNR distributions for summer (June-August) and winter (December-February) months. The centre of each rose diagram corresponds to the centre of the seismic network.

**Table 1.** Quantitative comparison of summer and winter $B(\theta)$ distributions. For each coda window, the table gives the summer–winter Pearson correlation coefficient, summer/winter peak azimuths, winter peak shift relative to summer, and winter/summer peak-amplitude ratio.

| Coda window | Summer–winter correlation | Summer/winter peak azimuth (°) | Winter peak shift relative to summer (°) | Winter/summer peak ratio |
|---|---|---|---|---|
| W1 | 0.78 | 285/285 | 0 | 1.14 |
| W2 | 0.84 | 255/285 | 30 | 1.21 |
| W3 | 0.72 | 255/285 | 30 | 1.54 |

The azimuthal noise-intensity distributions in Fig. 7 show that the dominant energy arrives mainly from the western to northwestern sector, consistent with the persistent influence of Atlantic microseism sources over Central Europe (Stehly et al., 2006). The summer and winter distributions are broadly similar across all three coda windows, indicating that the overall ambient-noise source geometry remains largely stable throughout the year. This similarity is supported quantitatively by the summer–winter correlations of $B(\theta)$, which range from 0.72 to 0.84 (Table 1). The dominant peak azimuth is unchanged in W1 and shifts by 30° in W2 and W3, while the winter/summer peak-amplitude ratios range from 1.14 to 1.54. These results indicate that winter noise amplitudes are enhanced, particularly at later coda lapse times, but that the overall directional pattern remains

https://doi.org/10.5194/egusphere-2026-3274
Preprint. Discussion started: 19 June 2026


broadly stable between seasons. Therefore, the seasonal differences in $B(\theta)$ are interpreted mainly as amplitude changes rather than a major reorganisation of the ambient-noise source field. This suggests that seasonal changes in ambient-noise directionality are unlikely to dominate the observed $\delta v/v$ variations, which are instead interpreted primarily as medium-related velocity changes rather than artefacts caused by seasonal changes in ambient-noise illumination (Weaver et al., 2009, Froment et al., 2010).

## 5 Discussion

The analysis of $\delta v/v$ variations across the Western Bohemia region demonstrates that, among the environmental variables considered, temperature exhibits consistently the strongest and physically interpretable coupling with $\delta v/v$. Temperature–$\delta v/v$ coherences are high in all three coda windows, with $\delta v/v$ lagging temperature by approximately 3 weeks. Such temporal offsets are fully consistent with thermoelastic forcing, in which seasonal surface temperature changes diffuse into the upper crust, generating delayed volumetric stress and strain that modulate seismic velocities (Hillers et al., 2015). In the present case, however, the absence of robust non-thermal responses indicates that thermoelastic stresses overwhelmingly dominate the $\delta v/v$ behaviour of the crust in Western Bohemia. We observe a secondary influence of groundwater level fluctuations on $\delta v/v$ variations. A straightforward explanation is elastic hydrological loading associated with changes in the water column. By contrast, direct pore-pressure effects are expected to be strongest in the near surface (within the upper few hundred meters) and to diminish rapidly with depth, becoming small at the $\sim$4 km depths relevant to this study. However, the observed delay of roughly four months is inconsistent with pure loading, which should produce an essentially instantaneous elastic response.

A more plausible explanation for the lag observed in Figure 6c is hydraulic diffusivity, i.e., delayed pore-pressure transmission through a permeable crustal volume. Adopting the 1-D pressure-propagation scaling for an incompressible, isotropic, and homogeneous medium, $r = \sqrt{4\pi D t}$ (Shapiro et al., 1997), and using $r = 4$ km (the mean of our depth sensitivity, $\sim$2-6 km) and $t = 110$ days yields $D \approx 0.14\ \mathrm{m^2\,s^{-1}}$. This estimate is within a factor of two of the value reported by Parotidis et al. (2003) for western Bohemia ($D \approx 0.27\ \mathrm{m^2\,s^{-1}}$), and it would overlap that value if $r$ is closer to the upper end of our sensitivity range (since $D \propto r^2$). The inferred $D$ should therefore be viewed as an effective, bulk diffusivity rather than a unique material constant, given the strong dependence on the assumed propagation distance and the simplifying 1-D, homogeneous approximation. Even so, diffusivity alone does not resolve the sign of the observed cross-correlation: pore-pressure increases would typically be expected to reduce elastic moduli and produce a negative $\delta v/v$, whereas we observe a positive correlation. This sign mismatch suggests that the measured relationship may reflect a superposition of mechanisms—for example, hydrological loading could control the polarity (via crack closure), while diffusive pressure equilibration governs the phase delay—or that groundwater level is acting as a proxy for a broader hydrological state that covaries with other drivers. Discriminating among these possibilities will require additional constraints, ideally combining multiple wells, independent loading/strain estimates, and joint modelling of amplitude and phase (lag) across seasons and frequency bands, which is beyond the scope of this work.

To assess how environmental forcing influences $\delta v/v$, we examine cross-correlations computed separately for the low- and high-period bands. Across all variables, the correlations are coherent and persistent when focusing on longer periods

https://doi.org/10.5194/egusphere-2026-3274
Preprint. Discussion started: 19 June 2026


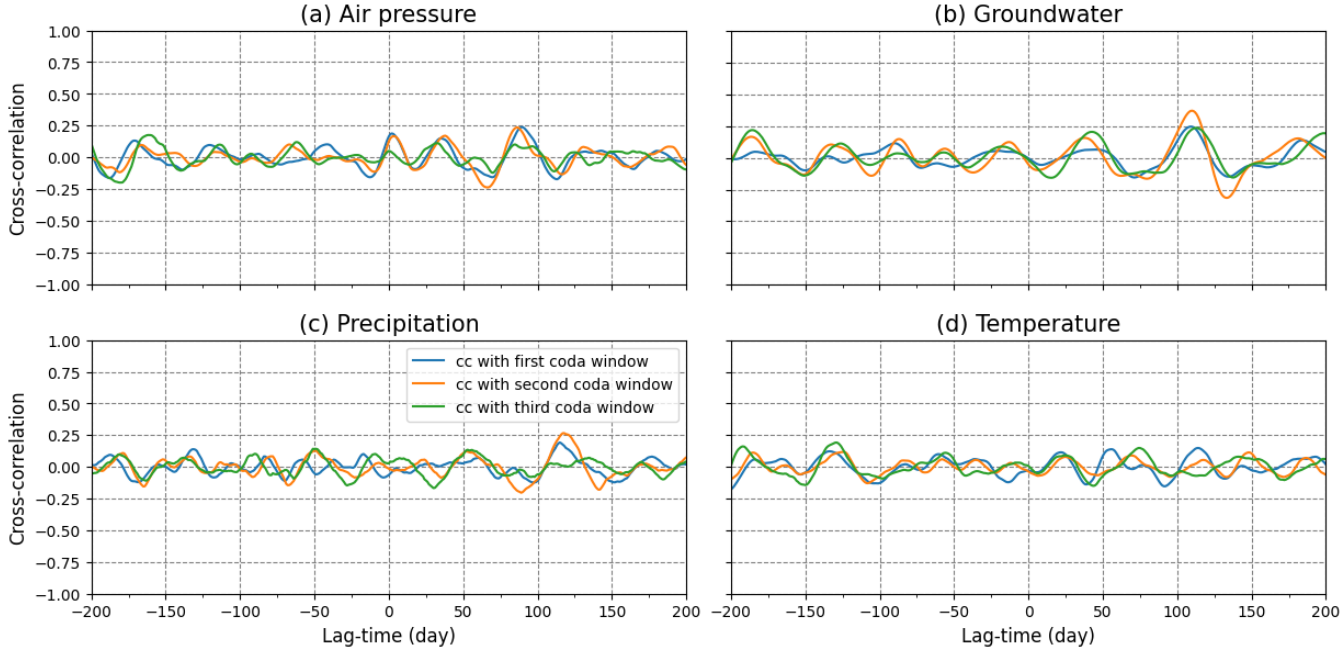


**Figure 8.** Cross-correlation estimations between $\delta v/v$ results (Fig. 3b) and the environmental factors : (a) atmospheric pressure,(b) groundwater level, (c) precipitation, (d) air temperature, after applying a highpass filter at 100-day.

(>100 days, Fig. S5), whereas they become weaker and more variable at shorter periods (<100 days, Fig. 8). However, the groundwater–$\delta v/v$ correlation retains a coherent feature around 110 days, the same lag-time observed in Fig. 6c, visible consistently across all three coda windows (Fig. 8b). Even though the amplitude of this 110-day feature is very small, its persistence across all three coda windows and its emergence after high-pass filtering indicate that it is not random noise. Thus, despite its small amplitude, the characteristic likely reflects a real, though weak, hydrological timescale inherent to the subsurface system rather than an artefact of the analysis.

The lack of highly robust coherence between $\delta v/v$ results and any environmental factors in this short-period range (Fig. 8) suggests that $\delta v/v$ fluctuations in these bands could be governed by internal crustal processes—such as microcrack evolution, stress redistribution associated with local seismicity, or small-scale changes in the scattering field—rather than by external environmental loading (Mikhael et al., 2024; Grêt et al., 2006; Cubuk-Sabuncu et al., 2021). Western Bohemia is characterised by episodic fluid migration, $CO_2$-rich degassing, and recurrent earthquake swarm activity, all of which can modify elastic properties within the crust through changes in pore pressure, crack opening and closure, and localised stress redistribution (Fischer et al., 2020; Woith et al., 2020; Bachura et al., 2021). Such processes are inherently irregular and do not follow fixed periodic cycles; therefore, their signatures tend to appear as broadband or weakly organised fluctuations in $\delta v/v$ rather than as discrete spectral peaks. Numerous studies have documented that fluid-driven stress perturbations in this region produce transient, non-periodic deformation responses (Bräuer et al., 2005, 2019; Fischer et al., 2017), and these mechanisms provide

https://doi.org/10.5194/egusphere-2026-3274
Preprint. Discussion started: 19 June 2026


a natural explanation for the lack of coherent forcing outside the dominant seasonal bands. In this context, the intermediate-period $\delta v/v$ variability likely reflects the combined effect of fluid-pressure changes and microstructural evolution in the crust, rather than any externally imposed environmental cycle.

The depth analysis indicates that all three coda windows used in this study are dominated by surface-wave energy, with the surface-wave contribution progressively decreasing from the first to the third window. Although the proportion of deeper penetrating body waves remains relatively small, it is not negligible. This interpretation is supported by the systematic decrease in $\delta v/v$ amplitude and correlation with the environmental factors from the first to the third coda window, even though the lag-time between $\delta v/v$ and the environmental factors remain broadly consistent. The earliest coda window is most sensitive to scattering paths that stay close to the source–receiver axis, thereby emphasising shallower crustal volumes where seasonal environmental fluctuation contrasts and associated strains are strongest. In contrast, later coda windows contain waves that have undergone multiple scattering and therefore sample increasingly larger and deeper regions that combine areas of both strong and weak environmental sensitivity. The observed reduction in amplitude, coupled with preserved coherence, is thus consistent with an environmental (e.g. atmospheric temperature and/or groundwater level) signal that is most pronounced in the shallow crust but remains detectable at greater depths, where it becomes attenuated and diluted by structural heterogeneity without fully disappearing (Richter et al., 2014).

Another important observation is the similarity of $\delta v/v$ behaviour across the three coda windows. Despite sampling different parts of the scattered wavefield and, by implication, different effective depth ranges, all coda windows show the same dominant long-period structure: the same annual and semi-annual peaks (Fig. 4), driven primarily by temperature, with comparable lags. This robust agreement indicates that the seasonal thermoelastic forcing is spatially extensive, influencing not only the very shallow crust but also deeper portions of the scattering volume. Previous ambient-noise studies have reported that seasonal $\delta v/v$ signals can be traced several kilometres into the crust, consistent with the penetration depth of thermal and associated stress perturbations (Meier et al., 2010; Ben-Zion and Alam, 2013). The inter-window consistency observed here supports a similar interpretation for Western Bohemia.

A key result is the dependence of $\delta v/v$ on interstation distance and azimuth. Seasonal cycles are much more clearly expressed in $\delta v/v$ estimates derived from the subset-stations than in those from the full set of station pairs. Short interstation distances enhance sensitivity to the shallow crust, where thermoelastic stresses are largest and most coherent, while long paths integrate over more heterogeneous and deeper structures, leading to spatial averaging that suppresses the seasonal signal. Additionally, the restriction to predominantly east–west oriented pairs improves cross-correlation stability, as these paths are better aligned with dominant ocean microseism directions that illuminate the interstation paths more uniformly (Stehly et al., 2006). The comparison between the full network and the path-selected subsets indicates that station geometry and path orientation strongly influence the stability of the recovered seasonal $\delta v/v$ signal. The subset with distances <20 km and azimuths of 60°-120° provides the clearest expression of the seasonal cycle, but similar temperature-related correlations are obtained for nearby distance and azimuth selections (Table S1). This suggests that the environmental interpretation is not an artefact of one narrowly tuned subset, although the selected subset provides the highest signal stability.

https://doi.org/10.5194/egusphere-2026-3274
Preprint. Discussion started: 19 June 2026


Taken together, these observations demonstrate that $\delta v/v$ in Western Bohemia is predominantly governed by seasonal thermoelastic strain, with possible contributions from groundwater level fluctuations at the periods where coherence is high. Path-dependent differences highlight the importance of station selection and wavefield illumination in recovering this signal, while inter-coda consistency suggests that the seasonal response is spatially coherent within the sampled scattering volume, although the present analysis does not provide a direct depth profile. The overall pattern indicates that $\delta v/v$ monitoring in this region primarily reflects the annual and semi-annual modulation of crustal elasticity by temperature, revealing a well-organised environmental control on seismic velocities that is observed consistently across the analysed coda windows and path selections.

## 6 Conclusions

In this study, we investigated seasonal seismic velocity variations in the western Bohemian Massif using four years of ambient-noise cross-correlations from 20 seismic stations. The $\delta v/v$ time series in the 0.1–0.5 Hz band show a clear annual cycle, with the most stable and coherent signals observed for station pairs shorter than 20 km and oriented between $60°$ and $120°$. This demonstrates that path length and azimuthal illumination strongly influence the recovery of seasonal $\delta v/v$ variations.

Lagged correlations with environmental variables indicate that atmospheric temperature is the dominant control on the observed seasonal velocity changes. The $\delta v/v$ response lags temperature by approximately 3 weeks, consistent with a thermoelastic mechanism. Groundwater-level fluctuations show a weaker positive correlation with a lag of about 110 days, but the underlying mechanism remains ambiguous because the positive polarity and long delay are difficult to explain using a single hydrological process. Precipitation and atmospheric pressure show weaker and less stable relationships with $\delta v/v$.

The decrease in amplitude and correlation at later coda lapse times is consistent with reduced sensitivity to shallow seasonal forcing and increased path averaging. However, because the measurements remain primarily surface-wave sensitive, the coda-window dependence should not be interpreted as a direct depth profile. Overall, the results show that ambient-noise monitoring can resolve environmentally driven velocity changes in the shallow crust of western Bohemia, provided that path geometry and noise-source illumination are carefully considered.

*Code and data availability.* The seismic data processed in this work were downloaded using the ObsPy FDSN client through the EIDA service infrastructure from the BGR node (Bundesanstalt für Geowissenschaften und Rohstoffe) and the LMU node (Ludwig-Maximilians-Universität München); and Bohemia Local Seismic Network (WEBNET). The temperature, precipitation and air pressure data used in this study were downloaded from Open-Meteo. The groundwater data were obtained from the national and regional portals ČHMÚ (2024), LfU (2026), and LfULG (2012). Geological map data were obtained from the Czech Geological Survey GeoČR50 service, the Saxony GK50 Erzgebirge/Vogtland service of the Sächsisches Landesamt für Umwelt, Landwirtschaft und Geologie, and the Bavarian dGK25 dataset of the Bayerisches Landesamt für Umwelt. The datasets were clipped and reclassified into common lithological groups for visualization. The sensitivity kernels shown in this study were derived using the python module DISBA. Processed $\delta v/v$ time series, station-pair metadata, environmental time series used for the correlation analysis, and analysis scripts will be made available in a FAIR-aligned public repository upon acceptance.

https://doi.org/10.5194/egusphere-2026-3274
Preprint. Discussion started: 19 June 2026


*Author contributions.* S. Mandal: Conceptualization, data processing, formal analysis, interpretation, visualization, and writing – original draft. T. Fischer: Conceptualization, Interpretation, Supervision, Project administration, Funding acquisition. B. Růžek: Conceptualization, Interpretation, Co-supervision.

*Competing interests.* The authors declare that they have no conflict of interest.

*Acknowledgements.* The work of Sourav Mandal and Tomáš Fischer was funded by the project SYNERGYS - systems for energy synergy, co-funded by the EU Operational Programme Just Transition, with grant No CZ.10.02.01/00/22_002/0000172. We thank Josef Vlček for his constructive feedback during the preparation of this manuscript.

https://doi.org/10.5194/egusphere-2026-3274
Preprint. Discussion started: 19 June 2026


## References

Adam, L. and Otheim, T.: Elastic laboratory measurements and modeling of saturated basalts, Journal of Geophysical Research: Solid Earth, 118, 840–851, https://doi.org/10.1002/jgrb.50090, 2013.

Aki, K. and Chouet, B.: Origin of coda waves: Source, attenuation, and scattering effects, Journal of Geophysical Research (1896-1977), 80, 3322–3342, https://doi.org/10.1029/JB080i023p03322, 1975.

Andajani, R., Tsuji, T., Snieder, R., and Ikeda, T.: Spatial and temporal influence of rainfall on crustal pore pressure based on seismic velocity monitoring, Earth, Planets and Space, 72, 177, https://doi.org/10.1186/s40623-020-01311-1, 2020.

Bachura, M., Fischer, T., Doubravová, J., and Horálek, J.: From earthquake swarm to a main shock–aftershocks: the 2018 activity in West Bohemia/Vogtland, Geophysical Journal International, 224, 1835–1848, https://doi.org/10.1093/gji/ggaa523, 2020.

Ben-Zion, Y. and Allam, A.: Seasonal thermoelastic strain and postseismic effects in Parkfield borehole dilatometers, Earth and Planetary Science Letters, 379, 120–126, https://doi.org/10.1016/j.epsl.2013.08.024, 2013.

Ben-Zion, Y. and Leary, P.: Thermoelastic strain in a half-space covered by unconsolidated material, Bulletin of the Seismological Society of America, 76, 1447–1460, https://doi.org/10.1785/BSSA0760051447, 1986.

Bensen, G., Ritzwoller, M., Barmin, M., Levshin, A., Lin, F., Moschetti, M., Shapiro, N., and Yang, Y.: Processing seismic ambient noise data to obtain reliable broad-band surface wave dispersion measurements, Geophysical Journal International, 169, 1239–1260, https://doi.org/10.1111/j.1365-246X.2007.03374.x, 2007.

Berryman, J. G.: Seismic waves in rocks with fluids and fractures, Geophysical Journal International, 171, 954–974, https://doi.org/10.1111/j.1365-246X.2007.03563.x, 2007.

Bettinelli, P., Avouac, J.-P., Flouzat, M., Bollinger, L., Ramillien, G., Rajaure, S., and Sapkota, S.: Seasonal variations of seismicity and geodetic strain in the Himalaya induced by surface hydrology, Earth and Planetary Science Letters, 266, 332–344, https://doi.org/10.1016/j.epsl.2007.11.021, 2008.

Beyreuther, M., Barsch, R., Krischer, L., Megies, T., Behr, Y., and Wassermann, J.: ObsPy: A Python Toolbox for Seismology, Seismological Research Letters, 81, 530–533, https://doi.org/10.1785/gssrl.81.3.530, 2010.

Birch, F.: The velocity of compressional waves in rocks to 10 kilobars: 1., Journal of Geophysical Research (1896-1977), 65, 1083–1102, https://doi.org/10.1029/JZ065i004p01083, 1960.

Brenguier, F., Shapiro, N., Campillo, M., Ferrazzini, v., Duputel, Z., Coutant, O., and Nercessian, A.: Toward forecasting volcanic eruption using seismic noise, Nature geoscience, 1, https://doi.org/10.1038/ngeo104, 2008.

Bräuer, K., Kämpf, H., Strauch, G., and Weise, S. M.: Isotopic evidence (3He/4He) of fluid-triggered intraplate seismicity, Journal of Geophysical Research: Solid Earth, 108, https://doi.org/10.1029/2002JB002077, 2003.

Bräuer, K., Kämpf, H., and Strauch, G.: Earthquake swarms in non-volcanic regions: What fluids have to say, Geophysical Research Letters, 36, https://doi.org/10.1029/2009GL039615, 2009.

(CHMI), C. H. I.: INSPIRE – Network of groundwater level monitoring objects, https://geoportal.gov.cz/php/micka/record/basic/5898879c-bbf8-429c-8cc4-0d56c0a80138?dlang=eng, metadata record; CC BY 4.0, 2024.

Christensen, N. I. and Wang, H. F.: The influence of pore pressure and confining pressure on dynamic elastic properties of Berea Sandstone, Geophysics, 50, 207–213, https://doi.org/10.1190/1.1441910, 1985.

https://doi.org/10.5194/egusphere-2026-3274
Preprint. Discussion started: 19 June 2026


Clarke, D., Zaccarelli, L., Shapiro, N. M., and Brenguier, F.: Assessment of resolution and accuracy of the Moving Window Cross Spectral technique for monitoring crustal temporal variations using ambient seismic noise, Geophysical Journal International, 186, 867–882, https://doi.org/10.1111/j.1365-246X.2011.05074.x, 2011.

Colombi, A., Chaput, J., Brenguier, F., Hillers, G., Roux, P., and Campillo, M.: On the temporal stability of the coda of ambient noise correlations, Comptes Rendus Geoscience, 346, https://doi.org/10.1016/j.crte.2014.10.002, 2014.

Cubuk-Sabuncu, Y., Jónsdóttir, K., Caudron, C., Lecocq, T., Parks, M. M., Geirsson, H., and Mordret, A.: Temporal Seismic Velocity Changes During the 2020 Rapid Inflation at Mt. Þorbjörn-Svartsengi, Iceland, Using Seismic Ambient Noise, Geophysical Research Letters, 48, e2020GL092 265, https://doi.org/10.1029/2020GL092265, 2021.

Fischer, T., Matyska, C., and Heinicke, J.: Earthquake-enhanced permeability – evidence from carbon dioxide release following the ML 3.5 earthquake in West Bohemia, Earth and Planetary Science Letters, 460, 60–67, https://doi.org/10.1016/j.epsl.2016.12.001, 2017.

Fischer, T., Vlček, J., and Lanzendörfer, M.: Monitoring crustal $CO_2$ flow : methods and their applications to the mofettes in West Bohemia, Solid Earth, 11, 983–998, https://doi.org/10.5194/se-11-983-2020, 2020.

Friedrich, A. M., Krüger, F., and Klinge, K.: Ocean-generated microseismic noise located with the Gräfenberg array, Journal of Seismology, 2, 47–64, 1998.

Froment, B., Campillo, M., Roux, P., Gouédard, P., Verdel, A., and Weaver, R. L.: Estimation of the effect of nonisotropically distributed energy on the apparent arrival time in correlations, Geophysics, 75, SA85–SA93, https://doi.org/10.1190/1.3483102, 2010.

für Umwelt (LfU), B. L.: Erklärung zur Barrierefreiheit (Accessibility statement) – Gewässerkundlicher Dienst Bayern, https://www.gkd.bayern.de/en/barrierefreiheit, 2023.

Gaebler, P. J., Eulenfeld, T., and Wegler, U.: Seismic scattering and absorption parameters in the W-Bohemia/Vogtland region from elastic and acoustic radiative transfer theory, Geophysical Journal International, 203, 1471–1481, https://doi.org/10.1093/gji/ggv393, 2015.

Gao, S. S., Silver, P. G., Linde, A. T., and Sacks, I. S.: Annual modulation of triggered seismicity following the 1992 Landers earthquake in California, Nature, 406, 500–504, https://doi.org/10.1038/35020045, 2000.

Gradon, C., Brenguier, F., Stammeijer, J., Mordret, A., Hindriks, K., Campman, X., Lynch, R., Boué, P., and Chmiel, M.: Seismic Velocity Response to Atmospheric Pressure Using Time-Lapse Passive Seismic Interferometry, Bulletin of the Seismological Society of America, 111, 3451–3458, https://doi.org/10.1785/0120210069, 2021.

Grêt, A., Snieder, R., and Scales, J.: Time-lapse monitoring of rock properties with coda wave interferometry, Journal of Geophysical Research: Solid Earth, 111, https://doi.org/10.1029/2004JB003354, 2006.

Heinicke, J., Braun, T., Alexandrakis-Zieger, C., and Buske, S.: Possible origin of the spatiotemporal evolution of the 2008 earthquake swarm in Northwest-Bohemia, Czech Republic, Physics of the Earth and Planetary Interiors, 333, 106 941, https://doi.org/10.1016/j.pepi.2022.106941, 2022.

Hennino, R., Trégourès, N., Shapiro, N. M., Margerin, L., Campillo, M., van Tiggelen, B. A., and Weaver, R. L.: Observation of Equipartition of Seismic Waves, Phys. Rev. Lett., 86, 3447–3450, https://doi.org/10.1103/PhysRevLett.86.3447, 2001.

Hillers, G., Ben-Zion, Y., Landès, M., and Campillo, M.: Interaction of microseisms with crustal heterogeneity: A case study from the San Jacinto fault zone area, Geochemistry, Geophysics, Geosystems, 14, 2182–2197, https://doi.org/10.1002/ggge.20140, 2013.

Hillers, G., Ben-Zion, Y., Campillo, M., and Zigone, D.: Seasonal variations of seismic velocities in the San Jacinto Fault area observed with ambient seismic noise, Geophysical Journal International, 202, 920–932, https://doi.org/10.1093/gji/ggv151, 2015.

Huenges, E., Erzinger, J., Kück, J., Engeser, B., and Kessels, W.: The permeable crust: Geohydraulic properties down to 9101 m depth, Journal of Geophysical Research: Solid Earth, 102, 18 255–18 265, https://doi.org/10.1029/96JB03442, 1997.

https://doi.org/10.5194/egusphere-2026-3274
Preprint. Discussion started: 19 June 2026


Institute of Geophysics, Academy of Sciences of the Czech Republic: West Bohemia Local Seismic Network, https://doi.org/10.7914/SN/WB, 1991.

Jiang, C. and Denolle, M. A.: NoisePy: A New High-Performance Python Tool for Ambient-Noise Seismology, Seismological Research Letters, 91, 1853–1866, https://doi.org/10.1785/0220190364, 2020.

Larose, E., Roux, P., Campillo, M., and Derode, A.: Fluctuations of correlations and Green's function reconstruction: Role of scattering, Journal of Applied Physics, 103, 114 907, https://doi.org/10.1063/1.2939267, 2008.

Li, H., Wang, D., Gao, J., Zhang, M., Wang, Y., Zhao, L., and Yang, Z.: Role of Saturation on Elastic Dispersion and Attenuation of Tight Rocks: An Experimental Study, Journal of Geophysical Research: Solid Earth, 125, https://doi.org/10.1029/2019JB018513, 2020.

Li, Y.-G., Vidale, J., Aki, K., Xu, F., and Burdette, T.: Evidence of shallow fault zone strengthening after the 1992 M7.5 Landers, California, Earthquake, Science (New York, N.Y.), 279, 217–9, 1998.

Li, Y.-G., Chen, P., Cochran, E., Vidale, J., and Burdette, T.: Seismic Evidence for Rock Damage and Healing on the San Andreas Fault Associated with the 2004 M 6.0 Parkfield Earthquake, Bulletin of The Seismological Society of America - BULL SEISMOL SOC AMER, 96, https://doi.org/10.1785/0120050803, 2006.

Lobkis, O. and Weaver, R.: Coda-Wave Interferometry in Finite Solids: Recovery of P -to- S Conversion Rates in an Elastodynamic Billiard, Physical review letters, 90, 254 302, https://doi.org/10.1103/PhysRevLett.90.254302, 2003.

Luu, K.: disba: Numba-accelerated computation of surface wave dispersion (v0.7.0). Zenodo., https://doi.org/10.5281/zenodo.14534395, 2024.

Malek, J., Brokešová, J., and Novotný, O.: New Velocity Structure of the Nový Kostel Earthquake-Swarm Region, West Bohemia, Determined by the Isometric Inversion, Pure and Applied Geophysics, 180, 1–24, https://doi.org/10.1007/s00024-023-03250-w, 2023.

Margerin, L., Campillo, M., Van Tiggelen, B. A., and Hennino, R.: Energy partition of seismic coda waves in layered media: Theory and application to Pinyon Flats Observatory, Geophysical Journal International, 177, 571–585, https://doi.org/10.1111/j.1365-246X.2008.04068.x, 2009.

Meier, U., Shapiro, N. M., and Brenguier, F.: Detecting seasonal variations in seismic velocities within Los Angeles basin from correlations of ambient seismic noise, Geophysical Journal International, 181, 985–996, https://doi.org/10.1111/j.1365-246X.2010.04550.x, 2010.

Mikhael, N., Poli, P., and Garambois, S.: Non-Linear Seismic Velocity Variations Observed During a Seismic Swarm in the Alto Tiberina Low Angle Normal Fault From Ambient Noise Correlation Measurements, Journal of Geophysical Research: Solid Earth, 129, e2023JB028 232, https://doi.org/10.1029/2023JB028232, 2024.

Nishimura, T., Uchida, N., Sato, H., Ohtake, M., Tanaka, S., and Hamaguchi, H.: Temporal changes of the crustal structure associated with the M6.1 earthquake on September 3, 1998, and the volcanic activity of Mount Iwate, Japan, Geophysical Research Letters, 27, 269–272, https://doi.org/10.1029/1999GL005439, 2000.

Obermann, A., Planes, T., Larose, E., Sens-Schonfelder, C., and Campillo, M.: Depth sensitivity of seismic coda waves to velocity perturbations of an elastic heterogeneous medium, Geophysical Journal International, 194, 372–382, https://doi.org/10.1093/gji/ggt043, 2013.

of Earth, D. and Environmental Sciences, Geophysical Observatory, U. o. M.: BayernNetz, https://doi.org/10.7914/SN/BW, 2001.

of Leipzig, U.: SXNET Saxon Seismic Network, https://doi.org/10.7914/SN/SX, 2001.

Pacheco, C. and Snieder, R.: Time-lapse travel time change of multiply scattered acoustic waves, The Journal of the Acoustical Society of America, 118, 1300–1310, https://doi.org/10.1121/1.2000827, 2005.

Parotidis, M., Rothert, E., and Shapiro, S. A.: Pore-pressure diffusion: A possible triggering mechanism for the earthquake swarms 2000 in Vogtland/NW-Bohemia, central Europe, Geophysical Research Letters, 30, https://doi.org/10.1029/2003GL018110, 2003.

https://doi.org/10.5194/egusphere-2026-3274
Preprint. Discussion started: 19 June 2026


Peng, Z. and Ben-Zion, Y.: Temporal Changes of Shallow Seismic Velocity Around the Karadere-Düzce Branch of the North Anatolian Fault and Strong Ground Motion, Pure and Applied Geophysics, 163, 567–600, https://doi.org/10.1007/s00024-005-0034-6, 2006.

Petrov, L. and Boy, J.-P.: Study of the atmospheric pressure loading signal in very long baseline interferometry observations, Journal of Geophysical Research: Solid Earth, 109, https://doi.org/10.1029/2003JB002500, 2004.

Planes, T., Larose, E., Margerin, L., Rossetto, V., and Sens-Schönfelder, C.: Decorrelation and phase-shift of coda waves induced by local changes: Multiple scattering approach and numerical validation, Waves in Random and Complex Media, 24, https://doi.org/10.1080/17455030.2014.880821, 2014.

Poli, P., Pedersen, H. A., and Campillo, M.: Emergence of body waves from cross-correlation of short period seismic noise, Geophysical Journal International, 188, 549–558, https://doi.org/10.1111/j.1365-246X.2011.05271.x, 2012.

Poupinet, G., Ellsworth, W. L., and Frechet, J.: Monitoring velocity variations in the crust using earthquake doublets: An application to the Calaveras Fault, California, Journal of Geophysical Research: Solid Earth, 89, 5719–5731, https://doi.org/10.1029/JB089iB07p05719, 1984.

Prawirodirdjo, L., Ben-Zion, Y., and Bock, Y.: Observation and modeling of thermoelastic strain in Southern California Integrated GPS Network daily position time series, Journal of Geophysical Research: Solid Earth, 111, https://doi.org/10.1029/2005JB003716, 2006.

Richter, T., Sens-Schönfelder, C., Kind, R., and Asch, G.: Comprehensive observation and modeling of earthquake and temperature-related seismic velocity changes in northern Chile with passive image interferometry, Journal of Geophysical Research: Solid Earth, 119, 4747–4765, https://doi.org/10.1002/2013JB010695, 2014.

Rodríguez Tribaldos, V. and Ajo-Franklin, J.: Aquifer Monitoring Using Ambient Seismic Noise Recorded With Distributed Acoustic Sensing (DAS) Deployed on Dark Fiber, Journal of Geophysical Research: Solid Earth, 126, https://doi.org/10.1029/2020JB021004, 2021.

Sabra, K. G., Gerstoft, P., Roux, P., Kuperman, W. A., and Fehler, M. C.: Extracting time-domain Green's function estimates from ambient seismic noise, Geophysical Research Letters, 32, https://doi.org/10.1029/2004GL021862, 2005.

Sato, H., Fehler, M. C., and Maeda, T.: Attenuation of High-Frequency Seismic Waves, pp. 153–184, Springer Berlin Heidelberg, Berlin, Heidelberg, https://doi.org/10.1007/978-3-642-23029-5_5, 2012.

Schimmel, M., Stutzmann, E., and Gallart, J.: Using instantaneous phase coherence for signal extraction from ambient noise data at a local to a global scale, Geophysical Journal International, 184, 494–506, https://doi.org/10.1111/j.1365-246X.2010.04861.x, 2011.

Sens-Schönfelder, C. and Wegler, U.: Passive image interferometry and seasonal variations of seismic velocities at Merapi Volcano, Indonesia, Geophysical Research Letters, 33, https://doi.org/10.1029/2006GL027797, 2006.

Shapiro, S. A., Huenges, E., and Borm, G.: Estimating the crust permeability from fluid-injection-induced seismic emission at the KTB site, Geophysical Journal International, 131, F15–F18, https://doi.org/10.1111/j.1365-246X.1997.tb01215.x, 1997.

Silver, P., Daley, T., Niu, F., and Majer, E.: Active Source Monitoring of Cross-Well Seismic Travel Time for Stress-Induced Changes, Bulletin of The Seismological Society of America - BULL SEISMOL SOC AMER, 97, 281–293, https://doi.org/10.1785/0120060120, 2007.

Stehly, L., Campillo, M., and Shapiro, N.: A study of the seismic noise from its long-range correlation properties, Journal of Geophysical Research : Solid Earth, 111, B10 306, https://doi.org/10.1029/2005JB004237, 2006.

Stehly, L., Campillo, M., and Shapiro, N. M.: Traveltime measurements from noise correlation: stability and detection of instrumental time-shifts, Geophysical Journal International, 171, 223–230, https://doi.org/10.1111/j.1365-246X.2007.03492.x, 2007.

Strollo, A., Cambaz, D., Clinton, J., Danecek, P., Evangelidis, C. P., et al.: EIDA: The European Integrated Data Archive and Service Infrastructure within ORFEUS, Seismological Research Letters, 92, 1788–1795, https://doi.org/10.1785/0220200413, 2021.

https://doi.org/10.5194/egusphere-2026-3274
Preprint. Discussion started: 19 June 2026


Sächsisches Landesamt für Umwelt, L. u. G. L.: WMS – Grundwasserstände und Quellschüttungen, https://metaver.de/trefferanzeige?docuuid=578e23a6-d69f-4620-a49a-ecc8c3799d41, lizenz: Datenlizenz Deutschland – Namensnennung – Version 2.0 (dl-de/by-2-0). Quellenvermerk: Quelle: Sächsisches Landesamt für Umwelt, Landwirtschaft und Geologie. Aktualisierung: fortlaufend., 2012.

Taira, T., Nayak, A., Brenguier, F., and Manga, M.: Monitoring reservoir response to earthquakes and fluid extraction, Salton Sea geothermal field, California, Science Advances, 4, e1701 536, https://doi.org/10.1126/sciadv.1701536, 2018.

Takano, T., Nishimura, T., Nakahara, H., Ohta, Y., and Tanaka, S.: Seismic velocity changes caused by the Earth tide: Ambient noise correlation analyses of small-array data, Geophysical Research Letters, 41, 6131–6136, https://doi.org/10.1002/2014GL060690, 2014.

Tsai, V. C.: A model for seasonal changes in GPS positions and seismic wave speeds due to thermoelastic and hydrologic variations, Journal of Geophysical Research: Solid Earth, 116, https://doi.org/10.1029/2010JB008156, 2011.

VanDam, T. M. and Wahr, J. M.: Displacements of the Earth's surface due to atmospheric loading: Effects on gravity and baseline measurements, Journal of Geophysical Research: Solid Earth, 92, 1281–1286, https://doi.org/10.1029/JB092iB02p01281, 1987.

VanDam, T. M., Blewitt, G., and Heflin, M. B.: Atmospheric pressure loading effects on Global Positioning System coordinate determinations, Journal of Geophysical Research: Solid Earth, 99, 23 939–23 950, https://doi.org/10.1029/94JB02122, 1994.

Wang, Q.-Y., Brenguier, F., Campillo, M., Lecointre, A., Takeda, T., and Aoki, Y.: Seasonal Crustal Seismic Velocity Changes Throughout Japan, Journal of Geophysical Research: Solid Earth, 122, 7987–8002, https://doi.org/10.1002/2017JB014307, 2017.

Weaver, R., Froment, B., and Campillo, M.: On the correlation of non-isotropically distributed ballistic scalar diffuse waves, The Journal of the Acoustical Society of America, 126, 1817–1826, https://doi.org/10.1121/1.3203359, 2009.

Weemstra, C., Boschi, L., Goertz, A., and Artman, B.: Seismic attenuation from recordings of ambient noise, Geophysics, 78, Q1–Q14, https://doi.org/10.1190/geo2012-0132.1, 2013.

Wegler, U. and Sens-Schönfelder, C.: Fault zone monitoring with passive image interferometry, Geophysical Journal International, 168, 1029–1033, https://doi.org/10.1111/j.1365-246X.2006.03284.x, 2007.

Woith, H., Daskalopoulou, K., Zimmer, M., Fischer, T., Vlček, J., Trubač, J., Rosberg, J.-E., Vylita, T., and Dahm, T.: Multi-Level Gas Monitoring: A New Approach in Earthquake Research, Frontiers in Earth Science, Volume 8 - 2020, https://doi.org/10.3389/feart.2020.585733, 2020.

Yang, Y., Ritzwoller, M. H., Levshin, A. L., and Shapiro, N. M.: Ambient noise Rayleigh wave tomography across Europe, Geophysical Journal International, 168, 259–274, https://doi.org/10.1111/j.1365-246X.2006.03203.x, 2007.

Yao, H. and Van Der Hilst, R. D.: Analysis of ambient noise energy distribution and phase velocity bias in ambient noise tomography, with application to SE Tibet, Geophysical Journal International, 179, 1113–1132, https://doi.org/10.1111/j.1365-246X.2009.04329.x, 2009.

Zigone, D., Ben-Zion, Y., Campillo, M., and Roux, P.: Seismic Tomography of the Southern California Plate Boundary Region from Noise-Based Rayleigh and Love Waves, Pure and Applied Geophysics, 172, 1007–1032, https://doi.org/10.1007/s00024-014-0872-1, 2015.

Zippenfenig, P.: Open-Meteo.com Weather API, https://doi.org/10.5281/zenodo.7970649, 2023.